Available online at www.sciencedirect.com
ScienceDirect
Biochimica et Biophysica Acta 1777 (2008) 331–342
Biochimica et Biophysica Acta BBA
www.elsevier.com/locate/bbabio

Influence of Histidine-198 of the D1 subunit on the properties of the primary electron donor, P_{680}, of photosystem II in *Thermosynechococcus elongatus*

Miwa Sugiura [a,*], Alain Boussac [b], Takumi Noguchi [c], Fabrice Rappaport [d]

[a] *Department of Plant Biosciences, School of Life and Environmental Sciences, Osaka Prefecture University, 1-1 Gakuen-cho, Naka-ku, Sakai, Osaka, 599-8531, Japan*
[b] *iBiTec-S, SB²SM, URA CNRS 2096, CEA Saclay, 91191 Gif sur Yvette, France*
[c] *Institute of Materials Science, University of Tsukuba, Tsukuba, Ibaraki 305-8573, Japan*
[d] *Institut de Biologie Physico-Chimique, Université Pierre et Marie Curie, UMR 7141 CNRS, 13 rue Pierre et Marie Curie, 75005 Paris, France*

Received 16 October 2007; received in revised form 7 January 2008; accepted 8 January 2008
Available online 26 January 2008

Abstract

The influence of the histidine axial ligand to the P_{D1} chlorophyll of photosystem II on the redox potential and spectroscopic properties of the primary electron donor, P_{680}, was investigated in mutant oxygen-evolving photosystem II (PSII) complexes purified from the thermophilic cyanobacterium *Thermosynechococcus elongatus*. To achieve this aim, a mutagenesis system was developed in which the *psbA*$_1$ and *psbA*$_2$ genes encoding D1 were deleted from a His-tagged CP43 strain (to generate strain WT*) and mutations D1-H198A and D1-H198Q were introduced into the remaining *psbA*$_3$ gene. The O_2-evolving activity of His-tagged PSII isolated from WT* was found to be significantly higher than that measured from His-tagged PSII isolated from WT in which *psbA*$_1$ is expected to be the dominantly expressed form. PSII purified from both the D1-H198A and D1-H198Q mutants exhibited oxygen-evolving activity as high as that from WT*. Surprisingly, a variety of kinetic and spectroscopic measurements revealed that the D1-H198A and D1-H198Q mutations had little effect on the redox and spectroscopic properties of P_{680}, in contrast to the earlier results from the analysis of the equivalent mutants constructed in *Synechocystis* sp. PCC 6803 [B.A. Diner, E. Schlodder, P.J. Nixon, W.J. Coleman, F. Rappaport, J. Lavergne, W.F. Vermaas, D.A. Chisholm, Site-directed mutations at D1-His198 and D2-His197 of photosystem II in *Synechocystis* PCC 6803: sites of primary charge separation and cation and triplet stabilization, Biochemistry 40 (2001) 9265–9281]. We conclude that the nature of the axial ligand to P_{D1} is not an important determinant of the redox and spectroscopic properties of P_{680} in *T. elongatus*.

Keywords: Photosystem II; P_{680}; Electron transfer; Chlorophyll axial ligand; Site-directed mutagenesis; *Thermosynechococcus elongatus*

1. Introduction

Photosystem II (PSII) is the enzyme responsible for photosynthetic oxygen evolution. The light-driven oxidation of water into dioxygen is catalyzed by a Mn_4Ca cluster which acts as both an accumulating device for oxidizing equivalents and the active site. All the cofactors involved in O_2 evolution are bound by the D1, D2, CP43 and CP47 proteins which are, themselves, part of a larger complex composed of more than 20 subunits [1,2].

Structural studies have confirmed that PSII contains two pigment branches across the membrane in a similar manner to that seen for bacterial reaction centre complexes [3]. The 2 chlorophylls, P_{D1} and P_{D2}, which constitute P_{680}, the primary

Abbreviations: CAPS, cyclohexylaminopropanesulfonic acid; Chl, chlorophyll; Chl_Z, redox-active chlorophyll in PSII; CP43, chlorophyll-binding protein; DCMU, 3-(3,4-dichlorophenyl)-1,1-dumethylurea; DCBQ, 2,6-dichloro-*p*-benzoquinone; EPR, electron paramagnetic resonance; FTIR, Fourier transform infrared; MES, 2-(*N*-morpholino) ethanesulfonic acid; Me_2SO; dimethyl sulfoxide; Pheo, pheophytin; PPBQ, phenyl-*p*-benzoquinone; PSII, photosystem II; P_{680}, primary electron donor; P_{D1}, P_{680} chlorophyll on D1; Q_A, primary quinone acceptor; Q_B, secondary quinone acceptor; TL, thermoluminescence; WT′, *T. elongatus* wild-type strain that has complete *psbA*$_1$, *psbA*$_2$ and *psbA*$_3$ genes and has a His-tag on the C terminus of CP43 (equivalent to 43-H strain); WT*, *T. elongatus* strain with a His-tag on the C terminus at CP43 and in which the *psbA*$_1$ and *psbA*$_2$ genes are deleted

* Corresponding author. Tel.: +81 72 254 9451; fax: +81 72 254 9918.
E-mail address: miwa@biochem.osakafu-u.ac.jp (M. Sugiura).

0005-2728/$ - see front matter © 2008 Elsevier B.V. All rights reserved.
doi:10.1016/j.bbabio.2008.01.007

electron donor, are in similar positions to the special pair of bacteriochlorophyll molecules; Chl_{D1} and Chl_{D2} are in analogous positions to the two accessory bacteriochlorophyll pigments and $Pheo_{D1}$ and $Pheo_{D2}$ are in equivalent locations to the two bacteriopheophytin molecules. A consensus is now emerging that primary charge separation in PSII occurs between Chl_{D1} and $Pheo_{D1}$ [4–6]. In a few ps, the $P_{680}^{+}Pheo_{D1}^{-}$ state is then formed with 80% of the cation residing on P_{D1} and 20% on P_{D2} [4]. Then, the pheophytin anion transfers the electron to a quinone, Q_A. P_{680}^{+} is reduced by Tyr_Z, at position 161 of the D1 protein. $Tyr_Z^{\cdot}$ is in turn reduced by the Mn_4Ca cluster.

An extraordinary feature of PSII amongst reaction centre complexes is the high redox potential of the P_{680}^{+}/P_{680} couple which is required to drive water oxidation, *e.g.* [7–9]. Possible reasons for the elevated value compared to Chl*a in vitro* include protein–pigment interactions, such as H-bonding, *e.g.* [10,11], pigment–cofactor interactions [12–16], a low dielectric environment [17] and puckering of pigment molecules [18], see [7–9,19] for general discussions.

The importance of the amino acid ligand, D1-His198, on the functional properties of P_{D1} has been examined by mutagenesis in the mesophilic cyanobacterium *Synechocystis* sp. PCC 6803 [20]. Of the 11 mutants examined only 3 were found to be photoautotrophic: H198Q, H198A and H198C mutants. Interestingly, in the D1-H198A mutant the Mg atom was conserved despite the lack of any proteinaceous ligand. The likely substitution of the His ligand by a water molecule had nevertheless some influence on the P_{680}^{+}/P_{680} absorption difference spectrum which was down-shifted by ≈2 nm in the Soret region. This spectroscopic change was accompanied by a decrease of ≈80 mV in the estimated midpoint redox potential. In the D1-H198Q mutant, in which glutamine could possibly act as a ligand to Mg, the P_{680}^{+}/P_{680} absorption difference spectrum was down-shifted by 3–4 nm in the Soret region but the redox potential was unchanged. Thus no obvious correlation between the spectral changes and the redox properties of P_{680} was found in these mutants [20].

In the *Synechocystis* sp. PCC 6803 mutant strains, most of the spectroscopic properties of P_{680} have been characterised in Mn-depleted PSII. It is well known, however, that the removal of the Mn-cluster alters the properties of P_{680}. For instance, the equilibrium constant of the electron transfer reaction between P_{680}^{+} and Tyr_Z increases by about two orders of magnitude upon Mn-depletion [21], possibly because of Coulombic interactions with the metal cluster [13]. This prompted us to study the role of the D1 axial ligand to P_{D1} in the thermophilic cyanobacterium *T. elongatus* from which fully active PSII can be purified and importantly for which the PSII structure is known [1, 2]. To achieve this aim we describe here the development of a mutagenesis system for the construction of D1 mutants in *T. elongatus* and the characterisation of D1-H198Q and D1-H198A mutants by low-temperature fluorescence, thermoluminescence, oxygen evolution, FTIR spectroscopy and time-resolved absorption spectroscopy.

2. Materials and Methods

2.1. Construction of the His_6-tag CP43, $\Delta psbA_1$, $\Delta psbA_2$ recipient strain (WT*)

A DNA fragment of approximately 4500 bp, including the open reading frames of the *psbA*$_1$ and *psbA*$_2$ genes and 1000 bp upstream and 1000 bp downstream of these two genes, was amplified by PCR (Expand High Fidelity PCR System, Boehringer Mannheim) and cloned into plasmid pUC19. A 2564-bp *Pst* I/*Sac* I

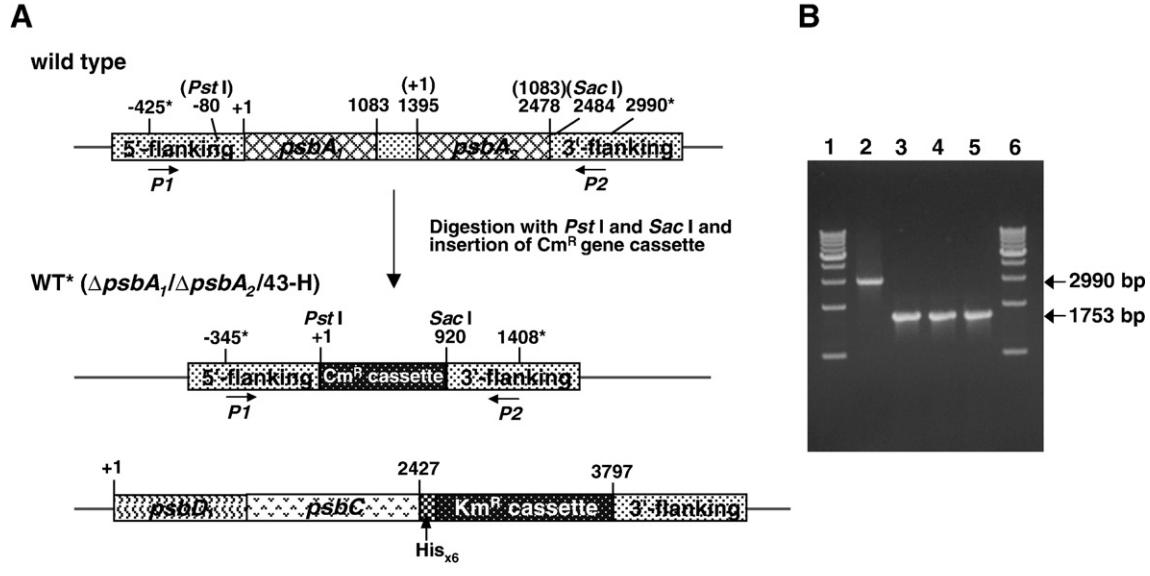

Fig. 1. (A) Map around the *psbA*$_1$ and *psbA*$_2$ genes in wild-type and deletion of both the *psbA*$_1$ and *psbA*$_2$ genes from the *T. elongatus* genome to produce WT*. A 2564-bp fragment which includes the *psbA*$_1$ and *psbA*$_2$ genes was replaced by a 920-bp fragment containing the Cm resistant cassette at *Pst* I and *Sac* I sites. Just before the stop codon of the *psbC* open reading frame, an additional DNA fragment encoding 6 consecutive histidine residues (His_{x6}) exists in WT*. *P1* and *P2* show positions of PCR primers to confirm the length of the *psbA*$_1$ and *psbA*$_2$ genes and/or the Cm resistant cassette. (B) Agarose gel (1%) electrophoresis of PCR amplification products using *P1* and *P2* primers. Lanes 1 and 6, 1 kb DNA ladder markers (Toyobo, Japan); lane 2, 43-H (WT′) strain; lane 3, WT* ($\Delta psbA_1/\Delta psbA_2$/43-H) strain; lane 4, D1-H198A strain; lane 5, D1-H198Q strain.

fragment which includes both $psbA_1$ and $psbA_2$ open reading frames was replaced by a 920-bp fragment containing the chloramphenicol (Cm) resistance gene, to generate plasmid pUCmA3. The *T. elongatus* strain, 43-H, which has a His-tag on the C-terminal end of CP43 [22], and a kanamycin (Km) resistance cassette downstream (Fig. 1A) was transformed with the plasmid pUCmA3. The CP43-His-tag, $psbA_1$/$psbA_2$ knocked out mutant (WT*) was selected by growth on Cm and Km, and its genotype was confirmed by PCR analysis using the *P1* primer (5′-ACAACTGCG-TATTTAGTTTTACTAACAATAA-3′) and *P2* primer (5′-GAAATCCAGCCCGT-CACGAGTGCTGGCGAT-3′) shown in Fig. 1A and B.

2.2. Construction of the D1-H198A and D1-H198Q mutants

The $psbA_3$ gene plus 5′- and 3′-flanking sequences was cloned from *T. elongatus* wild-type genomic DNA by PCR amplification and subcloned into plasmid vector pUC19. The nucleotide sequence was confirmed by sequencing by using a CEQ2000 DNA Analysis System (Beckman). A spectinomycin (Sp) and streptomycin (Sm) resistance gene cassette was inserted downstream of the stop codon of $psbA_3$. For making the D1-H198A and D1-H198Q site-directed mutants, the position around +595 of $psbA_3$ was modified by using a Quick-Change XL Site-Directed Mutagenesis Kit (Stratagene) as shown in Fig. 2A. Segregation of all the $psbA_3$ copies in genome of the deletion mutant was confirmed by digestion of $psbA_3$ with *Pvu* II after PCR amplification of the mutated region including the promoter region by using the *P3* (5′-CCAGG-CACTCAACTGGAGTTGTGAACGGTT-3′) and *P4* primers (5′-GCTGA-TACCCAGGGCAGTAAACCAGATGCC-3′) (Fig. 2B and C). Finally, the genomic DNA sequences including the mutated regions were confirmed by using a DNA sequencer. All the transformations of *T. elongatus* were done by elec-troporation (BioRad gene pulser). The segregated cells were selected as single colonies on DTN agar plates containing 25 μg of Sp mL^{-1}, 10 μg of Sm mL^{-1}, 40 μg of Km mL^{-1} and 5 μg of Cm mL^{-1} as previously described in [22–24].

2.3. Purification of thylakoids and PSII core complexes

The transformed cells were grown in 1 L cultures of DTN in 3-L Erlenmeyer flasks in a rotary shaker with a CO_2-enriched atmosphere at 45 °C under continuous light (≈80 μmol of photons m^{-2} s^{-1}). Thylakoids and PSII core complexes were

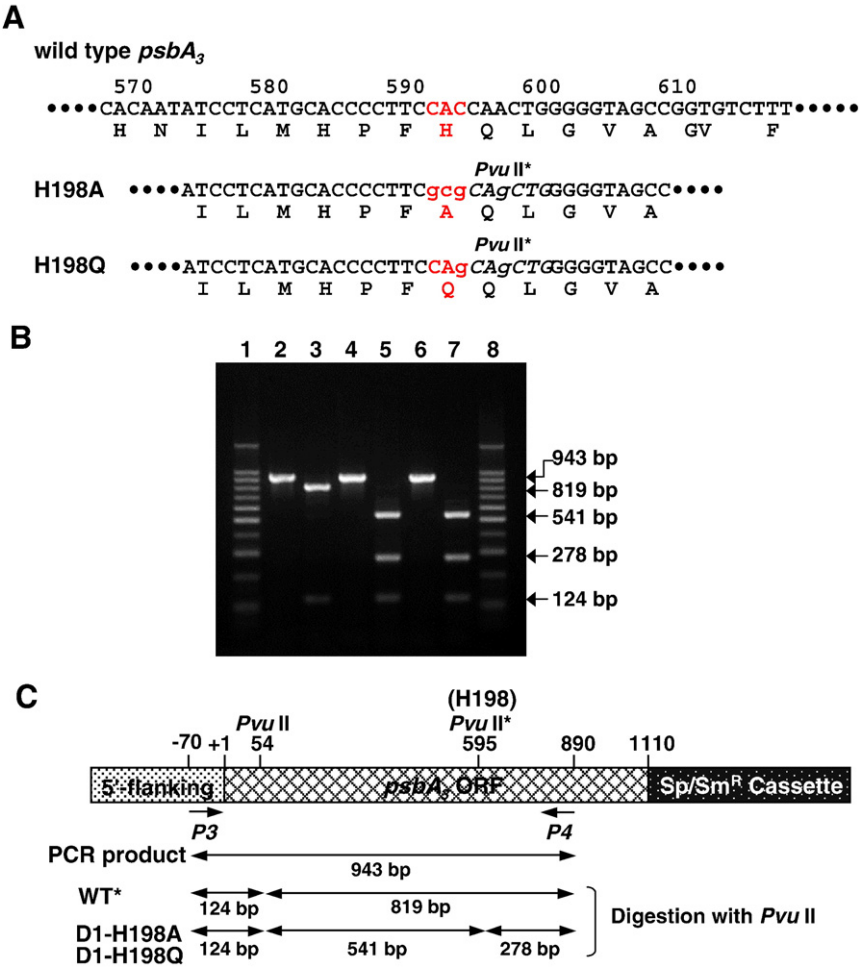

Fig. 2. Construction and confirmation of site-directed mutants strains D1-H198A and D1-H198Q in the $psbA_3$ gene. (A) Nucleotide sequence of $psbA_3$ and the deduced amino acid sequences around D1-H198 of WT*, D1-H198A and D1-H198Q. Positions H198, A198 and Q198 are indicated with red letters. Numbers correspond to the position from the initial codon. Substituted nucleotides are indicated in small letters. For the selection of mutants, the *Pvu* II recognition site (letters in italic) was created in D1-H198A and D1-H198Q. (B) Agarose gel (2%) electrophoresis of PCR amplification products by using the *P3* and *P4* primers (lanes 2, 4, and 6) and the products after digestion with *Pvu* II (lanes 3, 5, and 7). Lanes 1 and 8, 100 bp DNA ladder markers (Toyobo, Japan); lanes 2 and 3, WT* strain; lanes 4 and 5, D1-H198A strain; lanes 6 and 7, D1-H198Q strain. (C) Physical map around $psbA_3$ and theoretical DNA length after treating with *Pvu* II the PCR amplification products by using primers *P3* and *P4*. In the amplified region, the *Pvu* II site exists at position +54 in WT*, D1-H198A and D1-H198Q. The created *Pvu* II (shown as *Pvu* II*) site for H198 mutants is at position +595. Digestion of products from WT* with *Pvu* II generated fragments at 124-bp and 819-bp. Digestion of products from H198 mutants with *Pvu* II generated fragments at 124-bp, 541-bp and 278-bp as shown in B.

prepared as described earlier in [23,24]. The PSII core complexes bound to the Ni^{2+} resin were eluted with 200 mM L-histidine instead of imidazole to avoid unwanted ligation of the added imidazole to the Mg^{2+} ion of P_{680} Chl molecules in the D1-H198 mutants (during the washing step, the 15 mM imidazole was substituted for 2 mM L-histidine). PSII were concentrated by using Amicon Ultra-15 concentrator devices (Millipore) with a 100 kDa cut-off. Routinely, the total amount of Chl before the breaking of the cells was ≈150 mg, and the yield after PSII purification in terms of Chl amounts was ≈3–5%. PSII were stored in liquid nitrogen at a concentration of about 2 mg Chl mL^{-1} in a medium containing 10% glycerol, 1 M betaine, 15 mM $CaCl_2$, 15 mM $MgCl_2$, and 40 mM MES (pH 6.5) until use. Mn-depletion was done as previously described in [24]. For the experiment reported in Fig. 3, the samples were dark-adapted for 15 min at pH 6.5 in the medium indicated above. Then they were diluted in the same medium buffered at the indicated pH values with either CAPS or MES.

2.4. Oxygen evolution measurements

Oxygen evolution of PSII core complexes under continuous illumination was measured at 25 °C by polarography using a Clark-type oxygen electrode (Hansatech) with saturating white light at a Chl concentration of 5 μg of Chl mL^{-1} in the resuspending medium described above. A total of 0.5 mM DCBQ (2,6-dichloro-*p*-benzoquinone, dissolved in Me_2SO) was added as an electron acceptor. DCBQ reacts in the minute time range with betaine in the presence of O_2. For this reason, the PSII activity was measured immediately after the addition of DCBQ.

2.5. Fourier transform infrared (FTIR) measurements

FTIR spectra were measured as described in [25]. An aliquot (8 μL) of a suspension of the Mn-depleted PSII (by NH_2OH treatment [22]) (≈4.5 mg Chl mL^{-1}) in a pH 6.0 MES buffer (10 mM MES, 5 mM NaCl, and 0.06% *n*-dodecyl-β-maltoside) was mixed with 1 μL of 500 mM potassium ferricyanide and 1 μL of 10 mM SiMo, and loaded on a BaF_2 plate. The sample was then lightly dried under N_2 gas flow and covered with another BaF_2 plate with 0.7 μL of water. The sample temperature was adjusted to 265 K in a liquid-N_2 cryostat (Oxford, model DN1704) using a temperature controller (Oxford, model ITC-5). P_{680}^{+}/P_{680} FTIR difference spectra were recorded on a Bruker IFS-66/S spectrophotometer equipped with an MCT detector (D313-L). Scans in the dark (1 s) and under illumination (1 s) were repeated 4000 times. Averaged single-beam spectra were used to calculate light-*minus*-dark difference spectra. Light illumination was performed with continuous red light (≈16 mW cm^{-2} at the sample point) from a halogen lamp (Hoya-Schott HL150) equipped with a red cut-off filter (>600 nm). The spectral resolution was 4 cm^{-1}.

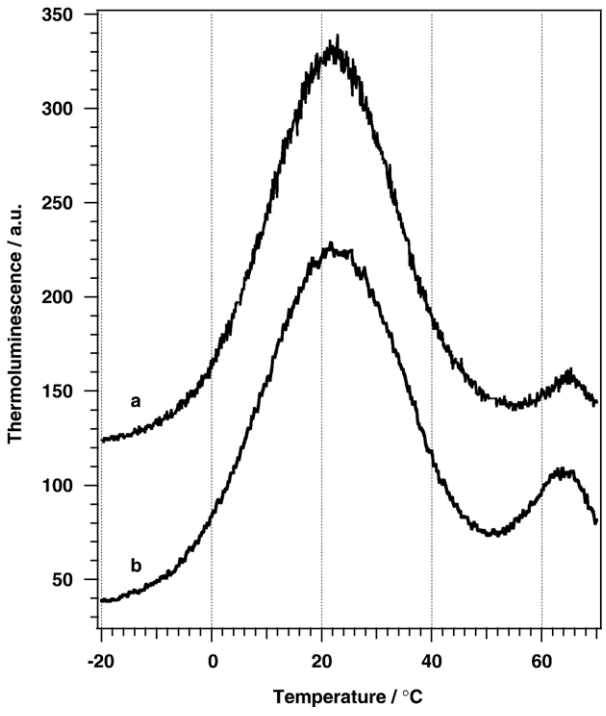

Fig. 3. Thermoluminescence glow curves from $S_2Q_A^-$ recombination. TL glow curves were recorded after one flash in PSII from WT′ (curve a) and PSII from WT* (curve b). DCMU was added on the dark-adapted PSII prior to the illumination.

2.6. UV-visible absorption change spectroscopy

Absorption changes were measured with a lab-built spectrophotometer [26] where the absorption changes are sampled at discrete times by short flashes. These flashes were provided by a neodymium:yttriumaluminum garnet (Nd:YAG) pumped (355 nm) optical parametric oscillator, which produces monochromatic flashes (1 nm full-width at half-maximum) with a duration of 6 ns. Excitation was provided by a dye laser pumped by the second harmonic of a Nd:YAG laser (685 nm, 1 mJ). PSII was used at 25 μg of Chl mL^{-1} in 10% glycerol, 1 M betaine, 15 mM $CaCl_2$, 15 mM $MgCl_2$, and 40 mM MES (pH 6.5). After dark-adaptation for 1 h at room temperature (20–22 °C), 0.1 mM phenyl-*p*-benzoquinone (PPBQ, dissolved in Me_2SO) was added as an electron acceptor.

2.7. Thermoluminescence measurements

Thermoluminescence (TL) glow curves were measured with a lab-built apparatus [27]. PSII core complexes were suspended in 40 mM MES buffer (pH 6.5) containing 10 mM NaCl, 15 mM $MgCl_2$, 15 mM $CaCl_2$, and 20% glycerol. The Chl concentration was 0.2 μg of Chl mL^{-1}. PSII were then dark-adapted for 1 h on ice. Just before loading the sample, 10 μM DCMU was added to a dark-adapted samples containing 15 μg of Chl. The samples were illuminated at 5 °C by using a saturating xenon flash (SL-230S; Sugawara, Japan) and then rapidly chilled to 77 K with liquid N_2. The frozen samples were then heated at a constant rate of 40 °C min^{-1} and TL emission was detected with a photomultiplier (Hamamatsu, R943-02).

2.8. Low-temperature fluorescence spectroscopy and room temperature absorption measurements

Fluorescence emission spectra were measured at 77 K using a Hitachi F-2500 Fluorescence Spectrophotometer (Tokyo, Japan). The whole cells were put on a 5 mm × 25 mm MF-Millipore™ membrane discs (pore size: 0.45 μm, Millipore). The cells were illuminated in liquid N_2 at 570 nm with a resolution of 20 nm. The fluorescence emission spectra were measured with a scan rate of 100 nm min^{-1} with a resolution of 2.5 nm. Absorption spectra were recorded at room temperature using a Hitachi U-2001 Spectrophotometer (Tokyo, Japan) with a scan rate of 100 nm min^{-1}. The samples were suspended in 40 mM MES buffer (pH 6.5) containing 10 mM NaCl, 15 mM $CaCl_2$ and 15 mM $MgCl_2$.

3. Results

3.1. Construction of a mutagenesis system for making D1 mutants in T. elongatus

There are three different *psbA* genes encoding the D1 protein in the *T. elongatus* genome [28], corresponding to tlr1843 (*psbA*$_1$), tlr1844 (*psbA*$_2$) and tlr1477 (*psbA*$_3$). When compared to the amino acid sequence of D1-3 ($PsbA_3$), the sequences of D1-1 ($PsbA_1$) and D1-2 ($PsbA_2$) differ by 21 and 31 amino acid residues, respectively. In the nucleotide sequences, 89 nucleotides of *psbA*$_1$ and 170 nucleotides of *psbA*$_2$ differ from the *psbA*$_3$ sequence. The initial codon of *psbA*$_2$ is located at 312 bp downstream of the terminal codon of *psbA*$_1$ (Fig. 1A, wild-type). In contrast, *psbA*$_3$ is independently located apart from *psbA*$_1$ and *psbA*$_2$ in the genome.

In order to create the D1-H198A and D1-H198Q mutants, the neighboring *psbA1* and *psbA2* genes were deleted and replaced by a chloramphenicol-resistance cassette and site-directed mutations were introduced into *psbA3*. In addition, the resulting strain also contained a His-tag at the C-terminal end of CP43 (WT′: this strain was originally named 43-H) [22] as shown in Fig. 1A. To thoroughly repress the expression of both *psbA1* and *psbA2*, the nucleotide region from −80 bp of *psbA1*, which is in the promoter region, to 6 bp downstream of the stop codon of *psbA2* was deleted. Neither the additional deletion of 80 bp in the promoter region of *psbA1* nor the deletion of 6 bp downstream of the *psbA2* stop codon must have functional effect since the two genes in the flanking regions i) tll1842 (encoding putative arsenical proton pump-driven ATPase) and ii) tll1845 (encoding hypothetical protein) are at 261 bp of the *psbA1* initial codon and at 83 bp of the *psbA2* stop codon, respectively. The P_{680} axial ligand mutants D1-H198A and D1-H198Q were constructed by introducing site-directed mutations into the *psbA3* gene of WT*. Fig. 1B shows an agarose gel electrophoresis of the PCR amplification DNA products from the genome of WT′, WT*, D1-H198A and D1-H198Q strains by using the *P1* primer (425-bp upstream of the *psbA1* initiation codon) and the *P2* primer (512-bp downstream of the *psbA2* stop codon) (positions in Fig. 1A). In the WT′ genome, a 2990-bp fragment was amplified (Fig. 1B, lane2). This fragment contained both the *psbA1* and *psbA2* open reading frames. In WT* and in the two D1-H198 mutants, a 1753-bp fragment was amplified which included the Cm resistant cassette instead of *psbA1* and *psbA2*. The absence of any DNA band at 2990 bp in WT* confirmed the complete removal of *psbA1* and *psbA2* (Fig. 1B, lanes 3 to 5).

3.2. Characterisation of PSII complexes isolated from WT*

PSII core complexes purified from the WT* strain exhibited an O_2 evolving activity of 5000–6000 μmol O_2 mg Chl^{-1} h^{-1}. Interestingly, this activity was consistently higher than that measured for His-tagged PSII isolated from a WT′ strain containing all three *psbA* genes (typically 3500–4500 μmol O_2 mg Chl^{-1} h^{-1}), in which *psbA1* is expected to be the most dominantly expressed form of D1 under the light intensity used in this work [29].

All the amino acid residues that act as ligands to the Mn_4Ca cluster [1,2] are conserved in the *psbA* gene products found in *T. elongatus*. Interestingly, amongst the 21 differences in primary structure, residue 130, which is within H-bonding distance to the 9-keto group of the $Pheo_{D1}$ chlorin ring, is a Gln in D1-1 but a glutamate in D1-3. In *Synechocystis* sp. PCC 6803 [30,31], a Gln residue at position 130 instead of a Glu residue decreases the energy gap between the $P^+_{680}Pheo^-_{D1}$ radical pair and P^*_{680} [30–33]. Consequently, the equilibrium constants of the P^*_{680} $Pheo_{D1}Q_A \leftrightarrow P^+_{680}Pheo^-_{D1}Q_A$ and $P^+_{680}Pheo^-_{D1}Q_A \leftrightarrow P^+_{680}Pheo_{D1}Q^-_A$ reactions are modified. These changes were evidenced by a longer lifetime of Q^-_A in the presence of DCMU as well as by an increase of the intensity of the thermoluminescence glow curve from the $S_2Q^-_A$ charge recombination with a Gln residue at position 130 [12,31–33]. The increase of the energy gap between the P^*_{680} and $P^+_{680}Pheo^-_{D1}$ couples, with Glu130 when compared to Gln130, was estimated to be ≈38 meV [30–33] *i.e.* a higher redox potential for $Pheo^-_{D1}/Pheo_{D1}$ that would favour the non-radiative $P^+_{680}Pheo^-_{D1} \rightarrow P_{680}Pheo_{D1}$ charge recombination at the expense of the radiative one which involves the repopulation of P^*_{680} [12,31–33].

Fig. 3 shows the thermoluminescence glow curves from the $S_2Q^-_A$ recombination in PSII isolated from WT′ and WT* *T. elongatus* strains. Assuming that $psbA_1$ is the gene dominantly expressed in WT′, the residue at position 130 of D1 in WT′ would be a Gln whereas in WT* it is necessarily a Glu residue. No significant differences were observed neither in the peak temperature of the glow curve nor in its intensity. In agreement with the results in Fig. 3, the $S_2Q^-_A$ recombination measured by following Q^-_A at 320 nm (see below) was also found similar in purified PSII from WT′ and WT* (not shown). The contrast between the results reported with the single Gln130 and Glu130 mutants and the present results may suggest that the Q130E substitution has almost no effect in *T. elongatus* when compared to the situation in *Synechocystis* sp. PCC 6803 or *Chlamydomonas reindhardtii*. Alternatively, either the 20 other additional substitutions may compensate the consequences of the Q130E substitution via long-range interactions (these long-range interactions could contribute to the thermostability of *T. elongatus*) or the expression level of

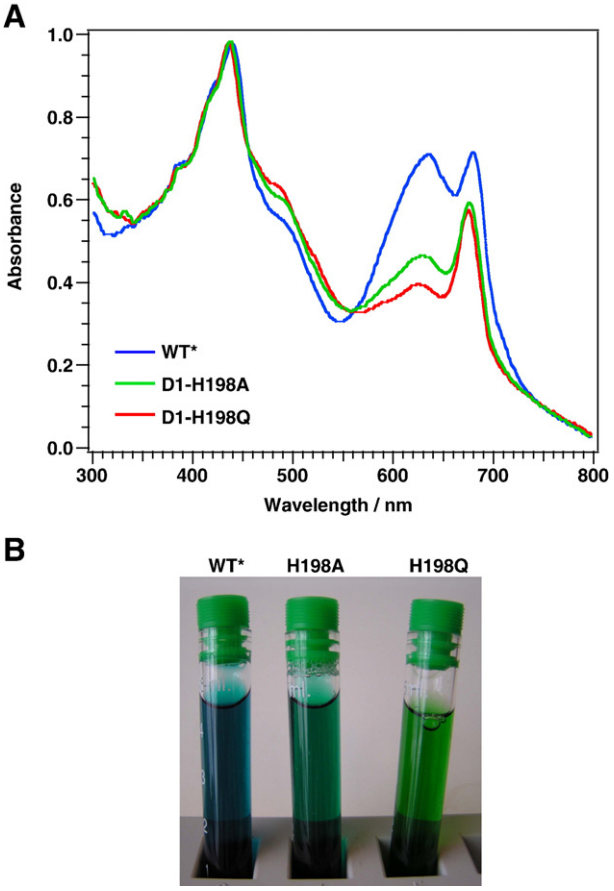

Fig. 4. (A) Room temperature absorption spectra of whole cells. Blue trace, WT*; red trace, green trace, D1-H198A, D1-H198Q respectively. The three curves were scaled at 430 nm. (B) Photo of supernatant fractions from broken cells.

the *psbA*$_3$ gene may be significant even in the WT′ strain, under the growth conditions used here.

3.3. Characterisation of the D1-H198A and D1-H198Q mutants

Both D1-H198A and D1-H198Q mutant cells were able to grow photoautotrophically. The generation time was ≈13 h in WT* and ≈15 h in D1-H198A and D1-H198Q mutant cells, respectively *i.e.* similar to the WT′ one. During the growth, the colour of the two D1-His198 mutants cells differed strongly from that of the WT* cells (Fig. 4A). Although both mutants showed an increased absorbance at 480 nm, reflecting a slight increase in the carotenoid content, the main difference between the mutant and WT* cells was observed at 630 nm. This indicated a decrease in either the content of phycocyanin or allophycocyanin (or both) in the D1-H198 mutants. The room temperature absorption spectrum of purified PSII was not modified by the mutations (not shown). Instead, as shown in Fig. 4B, the absorption of the phycobilisomes extracted from the D1-His198 mutants cells differed from those extracted from WT* cells. When compared to the WT*, the D1-H198Q mutant was more affected than the D1-H198A mutant.

These changes in the pigment composition were further investigated by measuring the energy transfer from the phycocyanin to PSII via allophycocyanin. Fig. 5 shows the 77 K fluorescence emission spectra in whole cells with the WT*, D1-H198A and D1-H198Q strains. The cells were cultivated under medium (≈80 μmol photons m^{-2} s^{-1}) (Fig. 5A) and low (≈15 μmol photons m^{-2} s^{-1}) light intensity (Fig. 5B). Under a light excitation at 570 nm, the main emission bands were at 645 nm (phycocyanin), 660 nm (allophycocyanin), 685 nm and 692 nm (PSII) and 725 nm (PSI). Amplitude of the fluorescence bands from allophycocyanin, PSII and PSI were much smaller in the mutants than in the WT* (Fig. 5A). PSII bands in both mutants appeared at 685 nm and 692 nm, whereas only the emission at 692 nm appeared in WT*. These results indicate that the energy transfer from allophycocyanin to PSII is not efficient in either of the D1-His198 mutants. Fig. 5B shows that the PSII to phycocyanin ratio was found to be higher in the two mutants than in the WT*. This is in a good agreement with the purification analysis which showed that the amount of PSII is ~1.5 fold larger in the mutants than in the WT*. The comparison of the amplitude of the $Tyr_D^{\bullet}$ and P_{700}^{+} EPR signals in thylakoids also indicated a higher PSII/PSI ratio in both mutants when compared to the WT* on an equal chlorophyll basis (not shown). It should be noted that the PSII fluorescence at 685 nm and 692 nm also slightly differed in the WT* and the mutants when the cells are cultivated under moderate light intensities (≈80 μmol photons m^{-2} s^{-1}) (Fig. 5B).

The characteristics of the D1-His198 mutants described above are very similar to the allophycocyanin-less mutant (knocked out *apcA* and *apcB*) and phycobilisome-linker less mutant (knocked out *apcE*) in *Synechocystis* sp. PCC 6803 [34,35]. One reason for such physiological effects could originate from a defective protection mechanism against excessive light. The secondary electron transfer pathway from cytochrome *b559* to P_{680}^{+} via carotenoid and Chl_Z [36–41] which is involved in the WT* could be affected and, in turn, alter the overall phycobilisome structure. Consistent with this hypothesis Fig. 5B shows that when the mutants and the WT* were cultivated under the low light conditions (≈15 μmol photons m^{-2} s^{-1}) the differences in the fluorescence emission spectra were less pronounced.

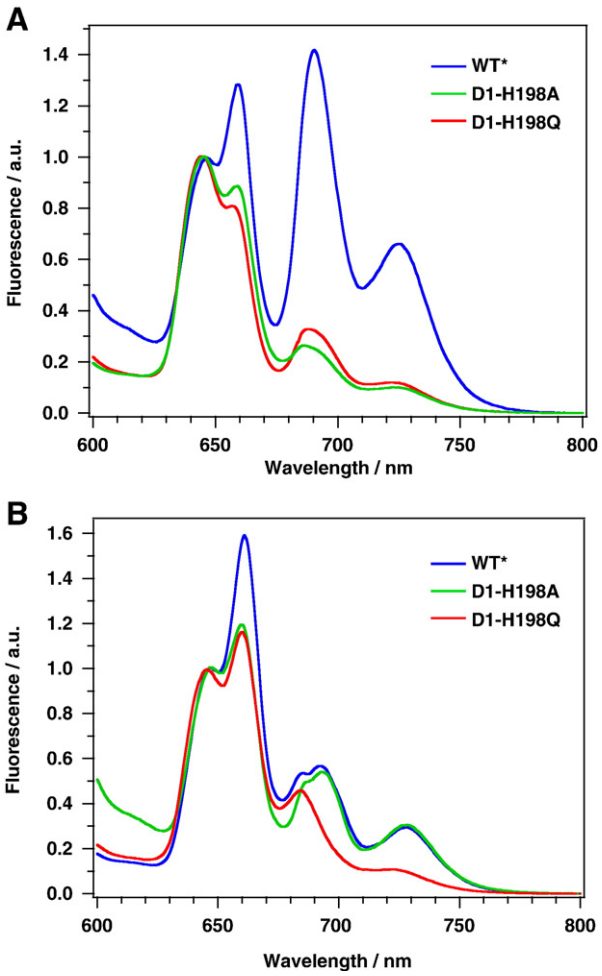

Fig. 5. Fluorescence emission spectra in whole cells at 77 K. The cells were cultivated either under a middle light intensity (80 μmol photons m^{-2} s^{-1}), Panel A, or a low light intensity (15 μmol photons m^{-2} s^{-1}), Panel B. WT* (blue spectrum,), D1-H198A (green spectrum) and D1-H198Q (red spectrum). The fluorescence spectra from the 3 strains were scaled to the phycocyanin fluorescence peak.

3.4. FTIR study of Mn-depleted PSII core complexes

Spectrum a in Fig. 6A shows the P_{680}^{+}/P_{680} FTIR difference spectrum (1780–1600 cm^{-1}) of WT* non-oxygen-evolving PSII. The prominent negative peak at 1700 cm^{-1} and a positive doublet at 1724 and 1710 cm^{-1} have been assigned to the 13^1-keto C=O stretching bands of neutral P_{680} and cationic P_{680}^{+}, respectively [23,25,42]. The single negative peak at 1700 cm^{-1} indicates that both keto C=O groups of neutral P_{680} are free from H-bonding [25]. The doublet peaks at 1724 and 1710 cm^{-1} have been interpreted as witnessing the predominant localization of the positive charge in P_{680}^{+} on one Chl molecule (70–80%) but partially shared with another Chl [25]. Smaller peaks in the 1750, 1743 and 1736 cm^{-1} arise from 13^2-ester C=O stretches [23,25,42]. Several

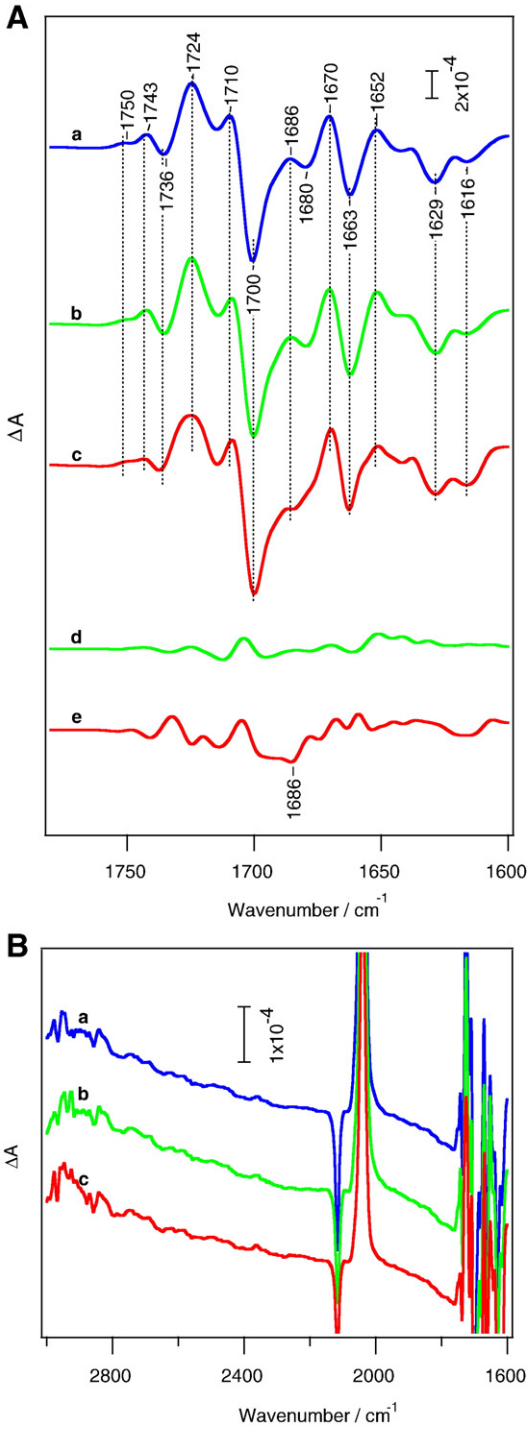

Fig. 6. (A) P^{+}_{680}/P_{680} FTIR difference spectra (1780–1600 cm^{-1}) of the Mn-depleted PSII core complexes of WT* (a, blue spectrum), D1-H198A (b, green spectrum) and D1-H198Q (c, red spectrum). Mutant-*minus*-WT* double difference spectra were shown for (d, green spectrum) D1-H198A and (e, red spectrum) D1-H198Q. (B) P^{+}_{680}/P_{680} spectra in the 3000–1600 cm^{-1} region showing the lower frequency part of a broad intervalence band of P^{+}_{680}. (a) WT*; (b) D1-H198A; (c) D1-H198Q.

bands at 1620–1680 cm^{-1} probably arise from the amide I bands of the protein backbone, which are induced upon cation formation. The negative peak at 1616 cm^{-1} can be assigned to the C=C vibration of the chlorin rings of P_{680} [25]. The partial charge delocalization over the Chl dimer in P^{+}_{680} has also been revealed by a broad intervalence band [43] at around 3000 cm^{-1} [25]. The lower frequency part of this broad feature was shown in spectra in Fig. 6B as a background increase above 1600 cm^{-1}.

In the P^{+}_{680}/P_{680} spectrum of the D1-H198A mutant (Fig. 6A, spectrum b), the above spectral features of WT* were virtually unchanged. This is also seen in the rather featureless (D1-H198A-*minus*-WT*) double difference spectrum (Fig. 6A, spectrum d). The observation that the keto C=O signal at 1724 and 1710 cm^{-1} and the broad feature above 1600 cm^{-1} of P^{+}_{680} (Fig. 6B, spectrum b) were kept unchanged indicates that the degree of charge delocalization over the dimer in P^{+}_{680} was not significantly affected by mutation. Thus, this observation provides solid evidence that the Chl molecule at P_{D1} was not replaced with a Pheo molecule in the D1-H198A mutant. Indeed, in bacterial reaction centre formation of a BChl-Pheo heterodimer resulted in a complete localization of the cation on the BChl side and consequently in the disappearance of a broad intervalence band and significant change in the keto C=O bands in P^{+}_{870}/P_{870} FTIR spectra [43,44].

The D1-H198Q mutant (Fig. 6A, spectrum c) also showed spectral features very similar to WT*, but some perturbations were observed. Although the positions of the keto C=O bands (1724/1710/1700 cm^{-1}) were virtually unchanged, the width of the 1724 cm^{-1} band was slightly broader than that of WT*. Also, a small positive peak at 1686 cm^{-1} in WT* was less clear in the D1-H198Q, suggesting that a negative peak exists at this position. These changes were more clearly seen in a D1-H198Q-*minus*-WT* double difference spectrum (Fig. 6A, spectrum e) showing a negative feature at 1686 cm^{-1} and several bands at 1750–1700 cm^{-1}. Since the Gln amide generally shows a C=O band at ~1680 cm^{-1} [45], this feature may arise from the Gln residue that was substituted for the His ligand of P_{D1}. Another possibility is that the structure of protein backbone was slightly perturbed by replacing His with Gln inducing some changes in the amide I vibration. On the other hand, the broad continuum feature above 1600 cm^{-1} did not change upon H198Q mutation (Fig. 6B, spectrum c). This observation together with the virtually unchanged keto C=O frequencies of P^{+}_{680} at 1724/1710 cm^{-1} (Fig. 6A, spectrum c) indicates that the charge distribution in P_{680} was not largely changed by this mutation.

3.5. Activity of oxygen-evolving complexes isolated from the D1-H198A and D1-H198Q mutants

The O_2 evolving activity of PSII purified from the D1-H198A and D1-H198Q strains were found similar to that of the WT* PSII when measured under saturating continuous illumination (typically 5000–6000 μmol O_2 mg Chl^{-1} h^{-1}). The intactness of the mutant PSII was further evidenced by the pattern of the flash-induced period four oscillations, when measured at 292 nm [46], which was similar to that measured in WT* PSII (not shown but see Supplementary material).

3.6. Time-resolved flash-induced absorption changes around 430 nm

In this spectral region, the redox changes of several species, such as the Chls, cytochromes, Tyr_Z and Q_A are associated

with absorption changes. The most prominent one however is associated with the formation of P_{680}^{+}. The P_{680}^{+}/P_{680} difference spectrum exhibits a strong Soret band bleaching in the 430 nm region. Fig. 7A shows the absorption changes from 411 to 455 nm in WT* PSII and in the D1-H198A and D1-H198Q PSII mutants. The absorption changes were measured 10 ns after the first flash, given to dark-adapted PSII *i.e.* in the S_1-state, and corresponded to the $P_{680}Q_A$ to $P_{680}^{+}Q_A^{-}$ transition. Although the spectra are not identical, the differences between the spectra obtained with the WT* and the mutants were rather weak. The D1-H198A mutant which exhibited a 1–2 nm blue-shift in *Synechocystis* sp. PCC 6803 [20] behaved similarly to the WT* in *T. elongatus* and the D1-H198Q mutant which was blue-shifted by about 3–4 nm in *Synechocystis* sp. PCC 6803 [20] is slightly red-shifted by ~0.5 nm, at most.

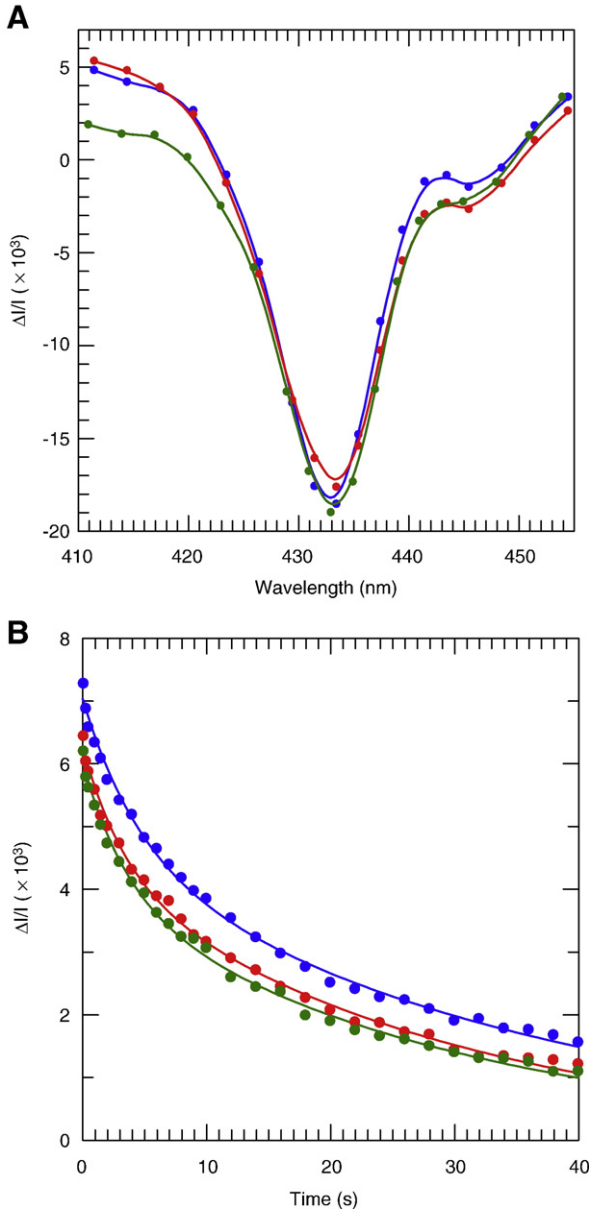

Fig. 7. Panel A; Difference spectra around 430 nm. The flash-induced absorption changes were measured in WT* PSII (blue trace), D1-H198Q PSII (red trace) and D1-H198A PSII (green trace) 15 ns after the first flash given on dark-adapted PSII. Upon dark-adaptation for 1 h at room temperature, 100 μM PPBQ (dissolved in Me_2SO) was added to the samples with Chl=25 μg mL^{-1}. Panel B; Kinetics of reoxidation of $QA^{\cdot -}$ reduction in the presence of DCMU. The flash-induced absorption changes were measured at 320 nm in WT* PSII (blue trace), D1-H198Q PSII (red trace) and D1-H198A PSII (green trace). Upon dark-adaptation of the samples (Chl=25 μg mL^{-1}) for 1 h at room temperature, 5 10^{-5} M DCMU were added. Then, following a saturating laser flash, the decay of $QA^{\cdot -}$ was followed by a train of detecting flashes at the indicated times.

3.7. Kinetic and energetic effects of the D1-H198 mutations in O_2 evolving PSII

Any change in the redox potential of the P_{680}^{+}/P_{680} couple is expected to induce a change in the P_{680}^{+} reduction by Tyr_Z and/or in P_{680} oxidation by $Tyr_Z^{\cdot}$. The former reaction can be followed by measuring the P_{680}^{+} reduction kinetics in the ns time range and the latter by measuring the $S_2Q_A^{-}$ charge recombination kinetics in the presence of DCMU. Alternatively, a change in the redox potential of the P_{680}^{+}/P_{680} couple can be assessed with thermoluminescence experiments by measuring the glow curve originating from the $S_2Q_A^{-}$ charge recombination in the presence of DCMU (Q band). To determine whether the redox potential of the P_{680}^{+}/P_{680} couple was affected by the mutation in *T. elongatus* we followed two different approaches.

First, the $S_2Q_A^{-}$ charge recombination was followed by measuring the transient absorption changes at 320 nm, where Q_A^{-} is the main contributor [47,48], after one flash given to dark-adapted PSII and in the presence of DCMU (Fig. 7B). No significant differences could be detected between the WT* PSII and D1-His198 mutants PSII.

Second, the thermoluminescence glow curve, in the presence of DCMU, resulting from the $S_2Q_A^{-}$ recombination was recorded in PSII isolated from WT* and from the D1-H198A and D1-H198Q mutants (Fig. 8). The amplitude of the glow curve was smaller in both mutants than in WT* PSII, and the peak of the glow curve was slightly up-shifted by 3 °C in the D1-H198Q mutant and down-shifted by 3 °C in the D1-H198A mutant.

3.8. Kinetics of P_{680}^{+} reduction in Mn-depleted PSII

Amongst the possibilities which could account for the different consequences of the D1-His198 mutations when introduced in *Synechocystis* sp. PCC 6803 or *T. elongatus*, we considered the fact that in the former case the Mn_4Ca cluster was absent in the isolated PSII complexes, whereas it is active in this study. We thus studied the reduction kinetics of P_{680}^{+} in Mn-depleted PSII from the *T. elongatus* WT* and D1-H198A and D1-H198Q strains. As shown in Fig. 9, the kinetics in the PSII from WT* and from the D1-H198 mutants were similar at each of the pH values examined. Yet, we noticed that they were significantly faster than those reported by Hays et al. from the study of the reduction of P_{680}^{+} in Mn-depleted PSII core complexes from a *Synechocystis* sp. PCC 6803 strain which contained only the *psbA-2* [49] or *psbA-3* gene (Diner and

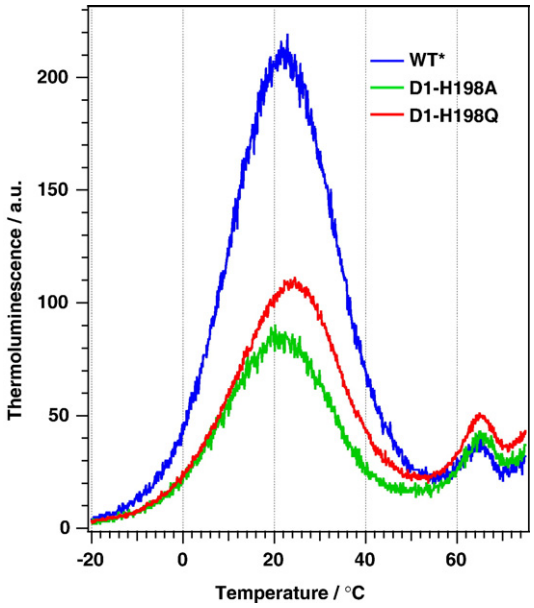

Fig. 8. Thermoluminescence glow curves from $S_2Q_A^-$ recombination. TL glow curves were recorded after one flash in PSII from WT* (blue curve), from D1-H198A (green curve) and D1-H198Q (red curve). DCMU was added on the dark-adapted PSII prior to the illumination.

Rappaport, unpublished). Because there is no correspondence between the numbering of the *psbA*$_i$ genes in *T. elongatus* and *Synechocystis* sp. PCC 6803, those in *Synechocystis* sp. PCC 6803 are denoted here *psbA-i* to avoid any confusion. As an example, at pH 9.3 the major decay component had a half-time of ≈70 ns in the case of the WT* from *T. elongatus* whereas it was ≈220 ns in the case of PSII from *Synechocystis* sp. PCC 6803 [49]. We have therefore compared the reduction kinetics of P_{680}^+ in PSII purified either from WT* or from WT′ (inset of Fig. 9). To this aim, we chose an alkaline pH (pH=9.3), for which the overall oxidation of Tyr_Z by P_{680}^+ is kinetically limited by the electron transfer rather than by proton transfer [49–51]. In the hundreds ns to μs time range, corresponding to the reduction of P_{680}^+ by Tyr_Z, the decay kinetics was faster when the D1 subunit is expressed from *psbA*$_3$, whereas WT′ PSII yielded similar kinetics as those found with Mn-depleted PSII from *Synechocystis* sp. PCC 6803. Interestingly the slow component developing in the hundred μs time was similar in all three cases.

4. Discussion

The D1-His198 mutations in *T. elongatus* were introduced into the *psbA*$_3$ gene in a recipient strain (WT*) in which both the *psbA*$_1$ and *psbA*$_2$ genes have been deleted and in which a His_6-tag was added to the C terminus of CP43. Both the D1-H198A and D1-H198Q mutants grew photoautotrophically. In whole cells, the mutations had almost no effect on the growth rate. Yet, a dramatic change was observed in the spectral characteristics of the phycobilisomes whereas the carotenoid's content was only slightly affected (Fig. 4). Both the absorption of the phycobilisomes and the energy transfer from the phycocyanin to PSII (Fig. 5) were modified. This suggests that maybe the phycocyanin but certainly the allophycocyanin content in the phycobilisomes were modified. Such a phenotype is similar to that already observed under a stress upon high-light illuminations in other cyanobacteria [52]. The possible changes in the rods and/or core stoichiometry observed in these mutants would make them an interesting material in the structure/function studies on the phycobilisome.

Despite these significant changes in the light-harvesting properties, the yield of PSII following purification suggested that the amount of PSII per cell was conserved. This differs slightly from the situation in *Synechocystis* sp. PCC 6803 in which the D1-H198A mutant contained only 50–60% of PSII when compared to the wild-type [20]. Fully active PSII in O_2 evolution could be purified from both mutant strains with no significant modifications in the miss parameter and in the S_1/S_0 ratio in dark-adapted samples. FTIR data of P_{680}^+/P_{680} recorded in Mn-depleted PSII confirmed the preservation of the Mg atom in the D1-H198A mutant despite the lack of ligand from the protein, suggesting that a water molecule provides the axial ligand in this case.

In order to address the question as to whether the thermodynamic properties of P_{680} are modulated by the nature of the axial ligand to P_{D1} in *T. elongatus* PSII we studied the decay of $S_2Q_A^-$ by charge recombination. Indeed, the decay of Q_A^- by charge recombination with the S_2 state is determined by a combination of different pathways which all involved high energy states of P_{680} (namely the excited state P_{680}^* or the cation P_{680}^+) [12,31,33]. Whereas thermoluminescence only probes the radiative pathways, the direct measure at 320 nm of the decay of Q_A^- probes all the possible routes. As a consequence

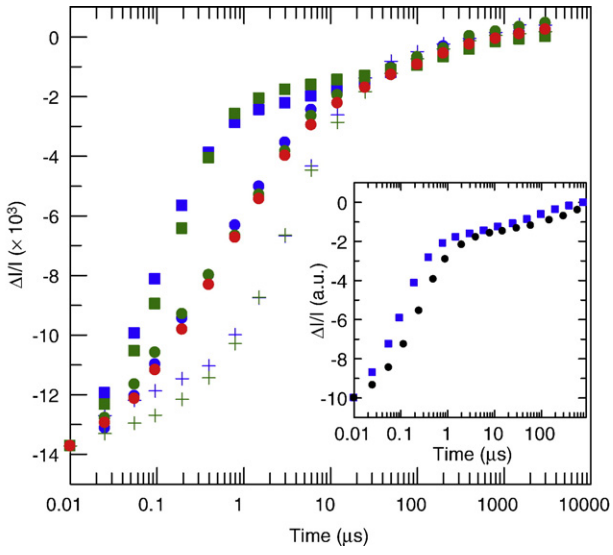

Fig. 9. Kinetics of P_{680}^+ reduction in Mn-depleted PSII. The flash-induced absorption changes were measured at 433 nm in WT* PSII (blue), D1-H198A (green) and D1-H198Q PSII (red). The dark-adapted samples were illuminated by 1 saturating flash, then the decay of P_{680}^+ was followed by a train of detecting flashes at the indicated times. Upon dark-adaptation for 15 min, 100 μM PPBQ (dissolved in Me_2SO) was added to the samples with Chl=25 μg mL^{-1}. The pH values were adjusted either with MES to 6.5 (circles) and to 5.6 (crosses) or with CAPS to 9.3 (squares). The inset shows the reduction of P_{680}^+ at pH 9.3 in the WT′ (black) and WT* (blue) at pH 9.3.

the rate of charge recombination, the intensity of the thermoluminescence glow curve and its peak temperature are correlated (see [12,31,33] and Supplementary material for further discussion).

In *Synechocystis* sp. PCC 6803, whereas the expected correlation between the peak temperature and amplitude of the thermoluminescence glow curve was nicely supported [31], in the case of the D1-Q130L and D1-Q130E mutations, which respectively down-shifted and up-shifted the midpoint potential of the Pheo/Pheo$^{\cdot-}$ couple, such a correlation was not observed for the D1-His198 mutants in which the midpoint potential of the P_{680}^{+}/P_{680} couple was affected [20]. Indeed, although the amplitude of the glow curve increased in the D1-H198K mutant and decreased in the D1-H198A mutant, the peak temperature increased in both mutants [31]. Moreover, in the case of D1-H198Q mutant in which the P_{680}^{+}/P_{680} redox potential is not or slightly up-shifted [20] the amplitude increased but the peak temperature decreased [31]. Yet, in the case of all the 5 mutants (Q130E, Q130L, H198A, H198Q, H198K) an increase (decrease) in the rate of charge recombination was systematically mirrored by a decrease in (increased) amplitude of the glow curve, so that we consider this correlation as robust. In this respect the finding that, in the case of the D1-His198 mutants from *T. elongatus*, the amplitude of the glow curves was decreased whereas the recombination rates were hardly affected weakens the simple interpretation that the changes in amplitude of the glow curve solely reflect a change in the $P_{680}^{+}Q_A^{-} \leftrightarrow S_2Q_A^{-}$ equilibrium. Thus, although the thermoluminescence measurements are consistent with an increased in the free energy gap between P_{680}^{*} and P_{680}^{+}Pheo$^{\cdot-}$, we are reluctant to entirely ascribe this putative change to a change in the $P_{680}^{+}Q_A^{-} \leftrightarrow S_2Q_A^{-}$ equilibrium. We are thus left with different possibilities: either the initial amount of photoactive centres is decreased in the mutant samples (such an apparent decreased activity could be due to a larger fraction of centres in the Q_B^{-} state before addition of DCMU, which would eventually result in a fraction of closed centres and thus in smaller luminescence intensity); or the increase in ΔG_{PPh} reflects an up-shift in the energy level of P_{680}^{*} rather than a down-shift the P_{680}^{+}Pheo$^{\cdot-}$ energy level. This would be the case for example if the equilibrium between P_{680}^{*} and the antenna Chl was slightly affected as suggested by the different ratio of the PSII fluorescence at 685 nm and 692 nm in WT* and mutant PSII in Fig. 5B.

The outcome of these studies on the charge recombination kinetics is thus that, in *T. elongatus* PSII, the midpoint potential of the P_{680}^{+}/P_{680} is hardly affected by either of the D1-H198A or D1-H198Q mutations. Fig. 7A shows that the absorption changes in the Soret region of P_{680} upon oxidation in the purified O_2 evolving PSII from WT* and D1-His198 mutants were resilient as well to these changes in the axial ligand. This is reminiscent of the finding that the (P_{700}^{+}–P_{700}) difference spectrum varied independently of the chemical nature of the axial ligand [53]. In *Synechocystis* sp. PCC 6803 PSII, however, the D1-H198Q mutation induced a blue-shift by 3 nm of the (P_{680}^{+}–P_{680}) difference spectrum [20]. Since, these spectroscopic changes were obtained in Mn-depleted PSII, we also measured the (P_{680}^{+}–P_{680}) difference spectra in Mn-depleted PSII from WT* and D1-His198 mutants but detected no significant spectral changes (not shown). Therefore, the lack of significant modifications of the P_{680} properties in the D1-His198 mutants in *T. elongatus* was not a consequence of Mn_4Ca–P_{680} interactions.

This raises the issue of the possible reasons for the differences observed between *Synechocystis* sp. PCC 6803 and *T. elongatus* upon substitution of the D1-His198 axial ligand to P_{D1}. Comparison of the sequence of the D1 subunit encoded by the *psbA*$_3$ gene in *T. elongatus* and *psbA-3* gene in *Synechocystis* sp. PCC 6803 (note: this is the gene in which the mutations were introduced in *Synechocystis* sp. PCC 6803 [20]) does not point to any obvious candidate at the molecular level. Although in *T. elongatus* the D1 peptide sequences which are deduced from the *psbA* genes are not identical, in *Synechocystis* sp. PCC 6803 the sequences deduced from *psbA-2* and *psbA-3* are identical (see Supplementary material). Out of the various differences between the two subunits only three are non conservative and located in the relative vicinity to P_{680}: Ala152, Gln199, and Leu288 are found in *T. elongatus*, whereas Ser152, Met199 and Met288 are found in the *psbA-2* and *psbA-3* products in *Synechocystis* sp. PCC 6803. Residues at positions 152 and 288, however, are identical in all *psbA* gene products in *T. elongatus*. Yet, according to the X-ray structures [1,2], which were obtained with PSII containing the *psbA*$_1$ gene product, none of the side-chains of these residues directly interact with the P_{D1} chlorophyll. Would they, or one of them, have a role in determining the spectroscopic and/or redox properties of this chlorophyll, it is thus more likely to be indirect. Since the A152S or L288M substitution in *T. elongatus* and *Synechocystis* sp. PCC 6803 may provide hydroxyl or *S*-methyl groups possibly involved in H-bonds with neighboring side-chains, they may slightly constrain the scaffold which bears P_{D1} and P_{D2}. We note that, owing to the identity of *psabA*$_1$ and *psbA*$_3$ at this various positions, the X-ray structures may neither support nor weaken this hypothesis, so that testing it would require an extensive site-directed mutagenesis strategy.

However, the differences in the primary structure of the D1 subunit encoded by the *psbA-3* gene in *Synechocystis* sp. PCC 6803 and *psbA*$_3$ gene in *T. elongatus* may indeed translate into slightly different three dimensional structures. The finding that P_{D1} may accommodate the likely exchange of its His axial ligand by a water molecule is, however, in itself, surprising. Recent DFT calculations [54] have shown that the effect of His/water exchange as an axial ligand on the redox potential of Chl*a* strongly depends on the value of the dielectric constant (ε). For an $\varepsilon = 80$ the change was negligible whereas it could reach 200 mV for $\varepsilon = 1$. The dielectric constant within a protein can vary significantly and its evaluation is not straightforward, *e.g.* [55,56]. Nevertheless, one of the outcomes of these DFT calculations [54] is that a slightly higher value for the dielectric constant around P_{680} in *T. elongatus* than in *Synechocystis* sp. PCC 6803 would account for the lack of a modification of the P_{680} redox potential in the D1-H198A mutant. Again, the differences in the sequence of the D1 subunit in the two organisms may result in slightly different electrostatic

environments for P_{680}. Yet, these differences must be kept small enough to maintain the high oxidizing power of the $P_{680}^{+\cdot}$ state which would otherwise significantly decrease.

One can find other examples of the likely structural differences between D1 subunits encoded by the various *psbA* genes in the comparison of some of the electron transfer reactions involved in the PSII function. We found that the reduction of $P_{680}^{+\cdot}$ in the hundreds of ns to the μs time range in *T. elongatus* was faster in WT* PSII than in WT′ PSII and that the latter yielded similar kinetics as those found with Mn-depleted PSII from *Synechocystis* sp. PCC 6803. In the hundreds of μs time range which is usually ascribed to the $P_{680}^{+\cdot}Q_A^{-\cdot}$ recombination reaction, the similar half-time found is in agreement with the finding that the $P_{680}^{+\cdot}/P_{680}$ redox potential is similar in WT′ PSII and WT* PSII. Thus, the faster rate obtained for the reduction of $P_{680}^{+\cdot}$ reduction rather reflects a change in the properties of Tyr_Z and/or of the H-bond network which participates to the transfer of its phenolic proton upon its oxidation, than a change in the P_{680} properties.

Another example comes from the comparison of the $S_2Q_A^{-\cdot}$ charge recombination which is significantly slower in *T. elongatus* than in *Synechocystis* sp. PCC 6803 or even spinach PSII. Typically, it develops in the seconds and ten seconds time range in mesophilic organisms and in *T. elongatus*, respectively. Accordingly, the peak temperature of the thermoluminescence glow curve is up-shifted by ~15 °C in *T. elongatus*. Although, again, structural rationales for these differences are lacking, this points to small differences in the energetics of the various redox cofactors in PSII which most likely reflects subtle structural differences. In this context, the outcome of genetically engineered *T. elongatus* strains and controlled growth conditions promoting the expression of a single *psbA* gene may constitute the cornerstone to future project aimed at identifying these structural variations which likely exert a delicate tuning of the energetics of PSII.

Acknowledgements

This study was supported by the JSPS and CNRS under the Japan–France Research Cooperative Program for funding (to M.S. and F.R.), a grant from Nissan Science Foundation (to M.S.), Grant-in-Aid for Young Scientists (B) (18770116 to M.S.) and Grants-in-Aid for Scientific Research (17GS0314 and 18570145 to T.N.) from the Ministry of Education, Science, Sports, Culture and Technology. AB was in part supported by the Solar H program STRP from the European Community. We would like to thank Mr. Tatsunori Okubo for FTIR measurements, James Murray, James Barber, Peter Nixon, Masahiko Ikeuchi, Ghada Ajlani, Daniel Picot and Bill Rutherford for helpful discussions and Ms. Yu Matsuda for assistance with analyses of *T. elongatus* genomic DNA. We express thanks to Peter Nixon for reading and correcting the manuscript.

Appendix A. Supplementary data

Supplementary data associated with this article can be found, in the online version, at doi:10.1016/j.bbabio.2008.01.007.

References

[1] K.N. Ferreira, T.M. Iverson, K. Maghlaoui, J. Barber, S. Iwata, Architecture of the photosynthetic oxygen-evolving center, Science 303 (2004) 1831–1838.
[2] B. Loll, J. Kern, W. Saenger, A. Zouni, J. Biesiadka, Towards complete cofactor arrangement in the 3.0 A resolution structure of photosystem II, Nature 438 (2005) 1040–1044.
[3] U. Ermler, G. Fritzsch, S.K. Buchanan, H. Michel, Structure of the photosynthetic reaction-center from rhodobacter-sphaeroides at 2.65-angstrom resolution — cofactors and protein–cofactor interactions, Structure 2 (1994) 925–936 10.
[4] B.A. Diner, F. Rappaport, Structure, dynamics, and energetics of the primary photochemistry of photosystem II of oxygenic photosynthesis, Annu. Rev. Plant Biol. 53 (2002) 551–580.
[5] M.L. Groot, N.P. Pawlowicz, L.J. van Wilderen, J. Breton, I.H. van Stokkum, R. van Grondelle, Initial electron donor and acceptor in isolated photosystem II reaction centers identified with femtosecond mid-IR spectroscopy, Proc. Natl. Acad. Sci. U. S. A. 102 (2005) 13087–13092.
[6] A.R. Holzwarth, M.G. Muller, M. Reus, M. Nowaczyk, J. Sander, M. Rogner, Kinetics and mechanism of electron transfer in intact photosystem II and in the isolated reaction center: pheophytin is the primary electron acceptor, Proc. Natl. Acad. Sci. U. S. A. 103 (2006) 6895–6900.
[7] F. Rappaport, B.A. Diner, Primary photochemistry and energetics leading to the oxidation of the Mn_4Ca cluster and to the evolution of molecular oxygen in photosystem II, Coordination Chemistry Reviews 252 (2008) 259–272.
[8] G. Renger. Oxidative photosynthetic water splitting: energetics, kinetics and mechanism (2007) Photosynth. Res. in press. doi:10.1007/s11120-007-9185-x.
[9] G. Renger, A.R. Holzwarth, in: T.J. Wydrzynski, K. Satoh (Eds.), Photosystem II: the Light-Driven Water: Plastoquinone Oxidoreductase, Springer, Dordrecht, 2005, pp. 139–175.
[10] J.P. Allen, K. Artz, X. Lin, J.C. Williams, A. Ivancich, D. Albouy, T.A. Mattioli, A. Fetsch, M. Kuhn, W. Lubitz, Effects of hydrogen bonding to a bacteriochlorophyll–bacteriopheophytin dimer in reaction centers from *Rhodobacter-sphaeroides*, Biochemistry 35 (1996) 6612–6619.
[11] X. Lin, H.A. Murchison, V. Nagarajan, W.W. Parson, J.P. Allen, J.C. Williams, Specific alteration of the oxidation potential of the electron donor in reaction centers from *Rhodobacter sphaeroides*, Proc. Natl. Acad. Sci. U. S. A. 91 (1994) 1026510269.
[12] F. Rappaport, M. Guergova-Kuras, P.J. Nixon, B.A. Diner, J. Lavergne, Kinetics and pathways of charge recombination in photosystem II, Biochemistry 41 (2002) 8518–8527.
[13] H. Ishikita, W. Saenger, J. Biesiadka, B. Loll, E.W. Knapp, How photosynthetic reaction centers control oxidation power in chlorophyll pairs P_{680}, P_{700}, and P_{870}, Proc. Natl. Acad. Sci. U. S. A. 103 (2006) 9855–9860.
[14] N. Ginet, J. Lavergne, Interactions between the donor and acceptor sides in bacterial reaction centers, Biochemistry 39 (2000) 16252–16262.
[15] J. Alric, A. Cuni, H. Maki, K.V. Nagashima, A. Vermeglio, F. Rappaport, Electrostatic interaction between redox cofactors in photosynthetic reaction centers, J. Biol. Chem. 279 (2004) 47849–47855.
[16] H. Ishikita, B. Loll, J. Biesiadka, W. Saenger, E.W. Knapp, Redox potentials of chlorophylls in the photosystem II reaction center, Biochemistry 44 (2005) 4118–4124.
[17] K. Hasegawa, T. Noguchi, Density functional theory calculations on the dielectric constant dependence of the oxidation potential of chlorophyll: implication for the high potential of P_{680} in photosystem II, Biochemistry 44 (2005) 8865–8872.
[18] J. Fajer, Chlorophyll chemistry before and after crystals of photosynthetic reaction centers, Photosynth. Res. 80 (2004) 165–172.
[19] M. Grabolle, H. Dau, Energetics of primary and secondary electron transfer in photosystem II membrane particles of spinach revisited on basis of recombination-fluorescence measurements, Biochim. Biophys. Acta 1708 (2005) 209–218.
[20] B.A. Diner, E. Schlodder, P.J. Nixon, W.J. Coleman, F. Rappaport, J. Lavergne, W.F. Vermaas, D.A. Chisholm, Site-directed mutations at

D1-His198 and D2-His197 of photosystem II in *Synechocystis* PCC 6803: sites of primary charge separation and cation and triplet stabilization, Biochemistry 40 (2001) 9265–9281.
[21] H. Conjeaud, P. Mathis, The effect of pH on the reduction kinetics of P-680 in Tris-treated chloroplasts, Biochim. Biophys. Acta 590 (1980) 353–359.
[22] M. Sugiura, Y. Inoue, Highly purified thermo-stable oxygen-evolving photosystem II core complex from the thermophilic cyanobacterium *Synechococcus elongatus* having His-tagged CP43, Plant Cell Physiol. 40 (1999) 1219–1231.
[23] M. Sugiura, F. Rappaport, K. Brettel, T. Noguchi, A.W. Rutherford, A. Boussac, Site-directed mutagenesis of *Thermosynechococcus elongatus* photosystem II: the O_2-evolving enzyme lacking the redox-active tyrosine D, Biochemistry 43 (2004) 13549–13563.
[24] S. Un, A. Boussac, M. Sugiura, Characterization of the tyrosine-Z radical and its environment in the spin-coupled $S_2Tyr_Z^{\bullet}$ state of photosystem II from *Thermosynechococcus elongatus*, Biochemistry 46 (2007) 3138–3150.
[25] T. Okubo, T. Tomo, M. Sugiura, T. Noguchi, Perturbation of the structure of P_{680} and the charge distribution on its radical cation in isolated reaction center complexes of photosystem II as revealed by Fourier transform infrared spectroscopy, Biochemistry 46 (2007) 4390–4397.
[26] D. Béal, F. Rappaport, P. Joliot, A new high-sensitivity 10-ns time-resolution spectrophotometric technique adapted to in vivo analysis of the photosynthetic apparatus. Rev. Sci. Instrum. 70 (1999) 202–207.
[27] T. Noguchi, M. Katoh, Y. Inoue, A new system for detection of thermoluminescence and delayed fluorescence from photosynthetic apparatus with precise temperature control, Spectroscopy 16 (2002) 89–94.
[28] Y. Nakamura, T. Kaneko, S. Sato, M. Ikeuchi, H. Katoh, S. Sasamoto, A. Watanabe, M. Iriguchi, K. Kawashima, T. Kimura, Y. Kishida, C. Kiyokawa, M. Kohara, M. Matsumoto, A. Matsuno, N. Nakazaki, S. Shimpo, M. Sugimoto, C. Takeuchi, M. Yamada, S. Tabata, Complete genome structure of the thermophilic cyanobacterium *Thermosynechococcus elongatus* BP-1, DNA Res. 9 (2002) 123–130.
[29] P. B. Kós, Z. Deák, O. Cheregi, I. Vass, Differential regulation of psbA and psbD gene expression, and the role of the different D1 protein copies in the cyanobacterium *Thermosynechococcus elongatus*BP-1. Biochim. Biophys. Acta in press doi: 10.1016/j.bbabio.2007.10.015.
[30] S.A.P. Merry, P.J. Nixon, L.M.C. Barter, M.J. Schilstra, G. Porter, J. Barber, J.R. Durrant, D. Klug, Modulation of quantum yield of primary radical pair formation in photosystem II by site directed mutagenesis affecting radical cations and anions. Biochemistry 37 (1998) 17439–17447.
[31] K. Cser, I. Vass, Radiative and non-radiative charge recombination pathways in photosystem II studied by thermoluminescence and chlorophyll fluorescence in the cyanobacterium *Synechocystis* 6803, Biochim. Biophys. Acta 1767 (2007) 233–243.
[32] A. Cuni, L. Xiong, R.T. Sayre, F. Rappaport, J. Lavergne, Modification of the pheophytin midpoint potential in photosystem II: modulation of the quantum yield of charge separation and of charge recombination pathways. Phys. Chem. Chem. Phys. 6 (2004) 4825–4831.
[33] F. Rappaport, A. Cuni, L. Xiong, R. Sayre, J. Lavergne, Charge recombination and thermoluminescence in photosystem II, Biophys. J. 88 (2005) 1948–1958.
[34] A. Ghada, C. Vernotte, Phycobilisome core mutants of *Synechocystis* PCC 6803. Biochim. Biophys. Acta 1231 (1995) 189–196.
[35] G. Shen, S. Boussiba, W.F. Vermaas, *Synechocystis* sp PCC 6803 strains lacking photosystem I and phycobilisome function, Plant Cell 5 (1993) 1853–1863.
[36] D.H. Stewart, G.W. Brudvig, Cytochrome *b559* of photosystem II, Biochim. Biophys. Acta 1367 (1998) 63–87.
[37] A. Telfer, What is beta-carotene doing in the photosystem II reaction centre? Philos. Trans. R. Soc. Lond., B Biol. Sci. 357 (2002) 1431–1439.
[38] H.A. Frank, G.W. Brudvig, Redox functions of carotenoids in photosynthesis, Biochemistry 43 (2004) 8607–8615.
[39] C.A. Tracewell, J.S. Vrettos, J.A. Bautista, H.A. Frank, G.W. Brudvig, Carotenoid photooxidation in photosystem II, Arch. Biochem. Biophys. 385 (2001) 61–69.
[40] J. Hanley, Y. Deligiannakis, A. Pascal, P. Faller, A.W. Rutherford, Carotenoid oxidation in photosystem II, Biochemistry 38 (1999) 8189–8195.
[41] P. Faller, A. Pascal, A.W. Rutherford, Beta-carotene redox reactions in photosystem II: electron transfer pathway, Biochemistry 40 (2001) 6431–6440.
[42] T. Noguchi, T. Tomo, Y. Inoue, Fourier transform infrared study of the cation radical of P680 in the photosystem II reaction center: evidence for charge delocalization on the chlorophyll dimer, Biochemistry 37 (1998) 13614–13625.
[43] J. Breton, E. Nabedryk, W.W. Parson, A new infrared electronic transition of the oxidized primary electron donor in bacterial reaction centers: a way to assess resonance interactions between the bacteriochlorophylls, Biochemistry 31 (1992) 7503–7510.
[44] E. Nabedryk, S.J. Robles, E. Goldman, D.C. Youvan, J. Breton, Probing the primary donor environment in the histidineM200->leucine and histidineL173->leucine heterodimer mutants of *Rhodobacter capsulatus* by light-induced Fourier transform infrared difference spectroscopy, Biochemistry 31 (1992) 10852–10858.
[45] A. Barth, The infrared absorption of amino acid side chains, Prog. Biophys. Mol. Biol. 74 (2000) 141–173.
[46] J. Lavergne, Improved UV-visible spectra of the S-transitions in the photosynthetic oxygen-evolving system, Biochim. Biophys. Acta 1060 (1991) 175–188.
[47] J.P. Dekker, H.J. van Gorkom, M. Brok, L. Ouwehand, Optical characterization of photosystem II electron donors, Biochim. Biophys. Acta 764 (1984) 301–309.
[48] J. Lavergne, Optical difference spectra of the S-state transitions in the photosynthetic oxygen-evolving complex, Biochim. Biophys. Acta 894 (1987) 91–107.
[49] A.-M.A. Hays, I.R. Vassiliev, J.H. Golbeck, R.J. Debus, Role of D1-His190 in the proton-coupled oxidation of tyrosine YZ in manganese-depleted photosystem II. Biochemistry 38 (1999) 11851–11865.
[50] A.-M.A. Hays, I.R. Vassiliev, J.H. Golbeck, R.J. Debus, Role of D1-His190 in proton coupled electron transfer reactions in photosystem II: a chemical complementation study. Biochemistry 37 (1998) 11352.
[51] B.A. Diner, J.A. Bautista, P.J. Nixon, C. Berthomieu, R. Hienerwadel, R.D. Britt, W.F. Vermaas, D.A. Chisholm, Coordination of proton and electron transfer from the redox active tyrosine, YZ, of photosystem II and examination of the electrostatic influence of oxidized tyrosine, YD°(H+), Phys. Chem. Chem. Phys. 6 (2004) 4844.
[52] P. Nomsawai, N. Tandeau de Marsac, J.-C. Thomas, M. Tanticharoen, S. Cheevadhnrak, Light regulation of phycobilisome structure and gene expression in *Spirulina platensis* (*Arthrospira* sp. PCC 9438), Plant Cell Physiol. 40 (1999) 1194–1202.
[53] A.N. Webber, H. Su, S.E. Bingham, H. Kass, L. Krabben, M. Kuhn, R. Jordan, E. Schlodder, W. Lubitz, Site-directed mutations affecting the spectroscopic characteristics and midpoint potential of the primary donor in photosystem I, Biochemistry 35 (1996) 12857–12863.
[54] J. Heimdal, K.P. Jensen, A. Devarajan, U. Ryde, The role of axial ligands for the structure and function of chlorophylls, J. Biol. Inorg. Chem. 12 (2007) 49–61.
[55] S. Sinnecker, F. Neese, QM/MM calculations with DFT for taking into account protein effects on the EPR and optical spectra of metalloproteins. Plastocyanin as a case study, J. Comput. Chem. 27 (2006) 1463–1475.
[56] V.H. Teixeira, C.A. Cunha, M. Machuqueiro, A.S. Oliveira, B.L. Victor, C.M. Soares, A.M. Baptista, On the use of different dielectric constants for computing individual and pairwise terms in Poisson–Boltzmann studies of protein ionization equilibrium, J. Phys. Chem., B 109 (2005) 14691–14706.